IEEE Access
Multidisciplinary ⋮ Rapid Review ⋮ Open Access Journal

Received 10 February 2024, accepted 19 February 2024, date of publication 23 February 2024, date of current version 1 March 2024.

Digital Object Identifier 10.1109/ACCESS.2024.3369418

RESEARCH ARTICLE

Enhanced Fault Detection and Localization Strategy for High-Speed Protection in Medium-Voltage DC Distribution Networks Using Extended Kalman Filtering Algorithm

NAUMAN ALI LARIK, MENG SHI LI, AND QING HUA WU
School of Electric Power Engineering, South China University of Technology, Guangzhou 510641, China
Corresponding author: Meng Shi Li (mengshili@scut.edu.cn)

This work was supported by the Basic Research Plan, Basic and Applied Research Project of Guangzhou under Grant 202201010752.

ABSTRACT Conventional strategies are not effective in addressing the complex protection challenges in medium-voltage DC distribution networks (MVDCDN). The main challenge in MVDCDN is the high-rising DC fault current, requiring a robust and fast protection strategy. This paper proposes the use of an Extended Kalman filter (EKF) to detect various types of DC faults using only the current signal in the MVDCDN. In the first stage, current signals from the positive and negative poles corresponding bus are obtained. The EKF is then applied to the measured DC-current signals to generate two fault detection indices. The first index is the cumulative residuals (CR), calculated using the EKF iterative differencing process with updated current estimated state and noisy measurement. The second index is the modified DC version of total harmonic distortion, known as DC distortion factor (DCDF). The fault classification/zone identification (FCZI) unit is activated if changes in CR and DCDF are detected within the observation window of the relay. In the second stage, the FCZI unit calculates the Extended Kalman filter-based predicted energy (EKFBPE) for the faulty DC line section at both ends. The polarity of EKFBPE is used for fault classification and localization decisions. The proposed protection strategy requires low-band wireless communication capability in the smart grid. Extensive simulations using MATLAB ®Simulink 2022b are conducted on a ±2.5 kV MVDCDN with three feeders, considering various fault scenarios. The results demonstrate that the proposed scheme achieves 99.9% accuracy, under radial, looped, and meshed topology and is highly resilient to different types of faults with time of operation 1 msec. The scalability of proposed method and its effectiveness in handling higher voltage levels and associated fault uncertainty will investigate in future research.

INDEX TERMS Fault detection, fault zone identification, DC distribution networks, DC microgrids, extended Kalman filters.

I. INTRODUCTION

A. MOTIVATION AND PROBLEM STATEMENT

The incorporation of renewable energy sources into DC distribution networks represents an innovative development in modern power systems [1]. This integration intends to facilitate the shift to more sustainable and efficient electricity distribution with the help of solar or wind power. MVDCDNs have various benefits over conventional AC distribution networks [2]. However, the MVDCDN faces a number of issues in terms of protection and control [3]. More specifically, when a fault arises in an MVDCDN, the high fault current

The associate editor coordinating the review of this manuscript and approving it for publication was Qingchao Jiang.

rush to the fault's location may cause considerable hazards to network components, which could lead to damage or the entire system loss if not addressed swiftly [4]. Furthermore, diagnosing a negative pole-to-ground (NP-G) fault in an MVDCDN might be difficult because to low fault current and the absence of zero crossing [5]. As a result, a rapid protection approach is required to identify and mitigate the impact of faults in MVDCDN [6]. To avoid equipment damage and maintain network dependability, the protection scheme must respond to problems in milliseconds [7].

B. LITERATURE REVIEW

The existing literature review includes numerous protection methods for DC distribution networks. A quick DC microgrid fault diagnosis technique was suggested in [8], involving mathematical modeling and multi-objective optimization for fault identification/localization, while fault location is calculated by means of a genetic algorithm. Likewise, the authors in [9] offered a high-speed protection method employing mathematical morphology (MM). Which process energy signals from voltage and current measurements in a DC distribution line to speedily detect and classify faults based on polarity changes. Similarly, a local current-based fast HIF detection scheme for DC microgrid clusters using the MM was proposed in [10], employing two MM-based components: erosion filtering and regional maxima, providing reliable, cost-effective fault detection without communication channels. The authors in [11] presented a new scheme centered on fault-propagating traveling waves (TWs) to identify, categorize, and localize diverse DC fault types within MVDC distribution network. Other authors in [12] presented a new TW-based protection for hybrid DC transmission networks by analyzing TW propagation in the system. Reference [13] introduced a fault detection method for DC microgrids with electric vehicles and energy storage, combining dynamic mode decomposition and instantaneous frequency calculation using voltage and current signals to minimize transient effects. Similarly, authors in [14] suggested a fault detection technique for DC microgrids, merging dynamic mode decomposition and instantaneous frequency calculation from voltage and current signals to reduce transient impacts. Reference [15] presented a fault detection technique based on Teager energy on DC current signal at line ends. Moreover, the least square algorithm was used for fault location estimation by distinguishing internal and external faults in a simulated DC microgrid. A centralized distance protection unit with a two-stage relay process for fault detection and location was proposed in [16], utilizing the LoRaWAN protocol for relay communication. Reference [17] presented a local current-based algorithm for fault detection in a DC microgrid, using polarity and a central controller for backup operations during communication failure. A novel protection method for DC microgrids was presented in [18] based on Shannon entropy to evaluate current waveform information. The proposed method detected faults accurately despite noise and communication delays.

Some intelligent methods were also reported in previous work [19], [20]. Reference [21] introduced a fast-tripping protection scheme for DC microgrids, employing TWs and discrete wavelet transform (DWT) to detect high-frequency components of fault currents. Furthermore, it utilized a Support Vector Machine for fault type identification and Gaussian Process regression for fault location estimation. Reference [22] suggested a fault localization technique for DC microgrids via a pseudo-data-driven algorithm utilizing an analytical approach and model-based neural network. The [23] proposed an Online fault protection method for low-voltage DC microgrids using a transfer learning-based convolution neural network, achieving 99.78% accuracy in fault detection. A fault detection technique for DC microgrids using Wavelet transform on branch current measurements, employing Artificial Neural Networks was proposed in [24]. Reference [25] proposed a fault detection scheme for high-power loads in all-electric warships using wavelet transform and machine learning. Also enabling the identification of abnormal disturbances in load current profiles and validating the proposed scheme through real-time implementation on a Texas Instruments DSP, focusing on fault detection with potential for isolation once faults are diagnosed.

C. CONTRIBUTIONS

This research paper suggests the utilization of an Extended Kalman filter to detect different types of DC faults in the MVDCDN solely based on the current signal. The first step involves acquiring the current signals from the positive and negative poles associated with the bus. These signals are then subjected to the EKF, which generates two fault detection indices. The first index, known as CR, is calculated using the iterative differencing process of the EKF with updated current estimates and noisy measurements. The second index is a modified DC version of total harmonic distortion called DCDF. The FCZI unit is activated when changes in CR and DCDF are detected within the observation window of the relay. In the second stage, the FCZI unit computes the EKFBPE for the faulty DC line section at both ends. The polarity of EKFBPE is used to make decisions regarding fault classification and localization. Extensive simulations are conducted using MATLAB® Simulink 2022b on a ±2.5 kV MVDCDN with three feeders, considering various fault scenarios. The results indicate that the proposed scheme achieves a 99.9% accuracy rate with fast operation under radial, looped, and meshed topology and demonstrates high resilience against different fault types. Some remarkable value additions are as follows.

1. First-time novel utilization of EKF in MVDCDN for fault detection, classification, and localization in the time domain.
2. Only the current signal is utilized to generate novel CR, DCDF and EKFBPE indices. These indices are independent of fault type, and location.
3. The suggested protection strategy has the capability to identify high-resistance faults up to 50 ohms.

D. MANUSCRIPT ARRANGEMENT

The manuscript is further arranged in the following sections: Section II provides a detailed description of the utilized radial MVDCDN testbed. Basic mathematical modeling of the proposed scheme is mentioned in section III. Section IV elaborates the adapted methodology of the proposed scheme. Extensive results cases are illustrated in section V. Finally, the paper is concluded in section VI.

II. THE MVDCDN TEST-BED

The MVDCDN testbed utilized for fault analysis in the proposed technique is designed on MATLAB/Simulink 2022b. The single-line diagram of the MVDCDN is shown in **FIGURE** 1. Furthermore, four feeders; feeder-A, feeder-B, feeder-C, and feeder-D are connected to the main bus B0. The testbed comprises a total of eight buses B0 to B8. An IGBT-based three-level voltage source converter (VSC) is applied to connect the MVDCDN with the main AC grid at bus B0. At feeder-C and feeder-D, two photovoltaic (PV) distributed generation units of 2 MW each are linked through a DC/DC boost converter. The system operates at a voltage level of ±2.5 kV regulated by the VSC. The MVDCDN had two switches; switch-1 and switch-2 to obtain looped and meshed topological structure. Three DC loads are linked to buses B1, B2, and B8 via DC/DC buck converters, while two AC loads are connected at B5 and B6 utilizing an inverter. The DC line is represented by an RL model, disregarding capacitance. The DC line parameters include a resistance of 0.0273 Ω/km and an inductance of 0.0009337 Ω/km, with each section of the customized span. For fault detection, location, and classification, the designed relays are positioned at both ends of each DC line section.

III. BASIC MATHEMATICAL MODELING OF THE PROPOSED TECHNIQUE

The proposed method utilized an EKF for the detection classification and localization of different faults in MVDCDN. Therefore, this section mainly focused on the basic mathematical model for the designed EKF-based scheme.

A. OVERVIEW OF DC-CURRENT CHARACTERISTICS IN MVDCDN

Many research studies in the literature have focused on analyzing short-circuit scenarios in medium-voltage DC Distribution Networks. These studies align on the critical necessity of isolating the faulty section precisely during the capacitor discharging phase. This measure is vital to protect costly diodes and maintain the overall integrity of the distribution network. Moreover, the proposed protection scheme is reliant on CR, DCDF, and EKFBPE signal processing. Therefore, this section focuses on defining the basic current signal model involved in the computation of CR, DCDF, and EKFBPE. Eqs (1) and (2) provided below elucidate the swift rise in fault current and the simultaneous decline in voltage signal.

$$i_k = e^{-\omega_1 t} I_k / W_1 L + \sin \omega_k \tag{1}$$

And similarly,

$$v_k = e^{-\omega_1 t} V_k w_k / w_1 L_{line} + \sin(\omega_k + \beta) \tag{2}$$

where, i_k depicts the discrete value of current at k^{th} sample, while v_k depicts the discrete value of the voltage at k^{th} sample. Measured DC voltage and current signals during faulty conditions are presented in **FIGURE 2.** We know that in the proposed protection method we utilized the current signal only to extract the desired future for fault detection, classification, and localization.

Therefore, if a fault occurs at any line section of the MVDCDN, the fault current can be calculated using the eq (1) meanwhile this current contained some measurement noise "ℵ"and the eq (1) is re-equated as follows.

$$i_k = e^{-\omega_1 t} I_k / W_1 L + \sin \omega_k + \aleph \tag{3}$$

B. BACKGROUND AND PRINCIPLES OF EKF

In the proposed method the EKF was engaged for fault detection, phase identification and localization in MVDCDN. By utilizing the measurements from the MVDCDN buses and incorporating them into the filter's estimation algorithm. The step-by-step pseudo code of the EKF algorithm is mentioned in **TABLE 1.** The EKF has the ability to handle nonlinear systems and process measurements makes it a viable tool for the fault detection in DC distribution networks. The Extended Kalman Filter expands upon the traditional Kalman Filter to handle nonlinear systems. It focuses on estimating the state of a dynamic system during noisy measurements. This method involves two primary steps:

1. prediction and
2. update.

Initially, it estimates the system's state based on dynamics and the previous state estimate, followed by refining, and correcting this estimate using measurements. The EKF finds application across diverse fields such as signal processing, control systems, and navigation owing to its proficiency in handling nonlinear systems and accurately estimating states, even in the presence of uncertainties and noise. However, the discrete nonlinear noisy state-space current can be modeled as follows.

$$\widehat{y_{(k)}} = H\left(x_{(k)}\right)\left(i_{(k)}\right) = p_{(k)} + a_{(k)} + i_{(k)} \tag{4}$$

The measurement equation is depicted as.

$$x_{(k+1)} = \mathrm{f}(x_{(k)}) + \mathrm{G}(x_{(k)})(u_{(k)}) + w_k \tag{5}$$

These equations with some specialized initial states and parameterization are utilized by EKF for processing measured DC current signals in a utilized medium-voltage DC distribution network. Therefore, after the implementation of EKF pseudo code on the input eq (3), the estimated current obtained is as follow.

$$\hat{i_k} = \hat{I_k} + e \tag{6}$$

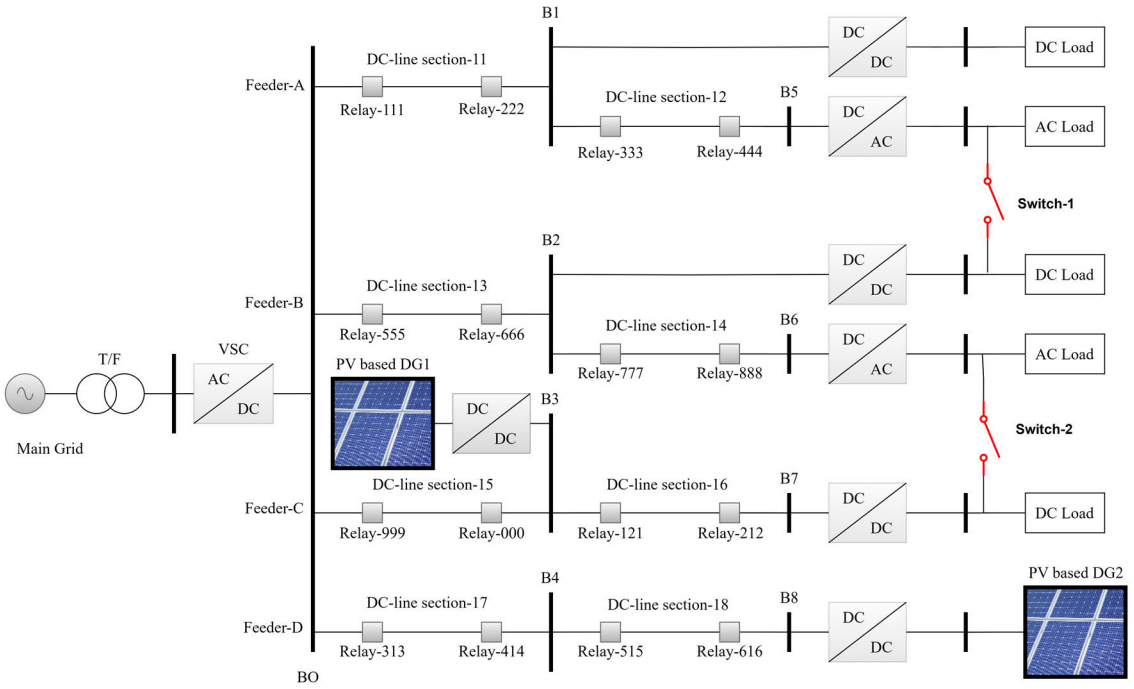

FIGURE 1. The MVDCDN testbed for fault analysis of the proposed scheme.

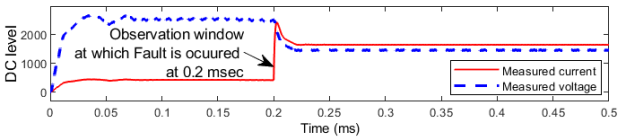

FIGURE 2. Measured current/voltage signal.

where, the $\hat{i}_k$ dipict the estimated current signal having $\hat{I}_k$ magnitude,and random error e. **FIGURE 3** illustrates the estimated current signature of EKF. Please note that this method provides an approximation of the integral and assumes a discrete representation of the continuous current signal over time. The rationale behind the choice of the EKF for fault detection in MVDCDN lies in its ability to effectively handle nonlinear and time-varying dynamic systems, characteristics often inherent in complex power distribution networks. Unlike traditional Kalman filters [26] [27], the extended version accommodates nonlinearities by linearizing system dynamics around an estimate, making it suitable for modeling the diverse behaviors of MVDCDN components under varying operating conditions and fault scenarios. Maintaining the stability and dependability of the MVDCDN relies heavily on the EKF's real-time fault identification, a recursive estimating technique critical for rapidly mitigating faults. In the presence of uncertainty, EKF's ability to offer accurate estimates and flexibility to dynamic situations make it an appealing alternative in MVDCDN for fault detection. This eventually improves system resilience and operating efficiency [28].

TABLE 1. Pseudo code of EKF.

From the perspective of node 1
Step 1: Initialization: Start by setting up initial parameters such as the state vector, covariance matrix, and noise parameters required for the EKF.
Step 2: Prediction Phase:
a. State Estimation: Predict the current system state using the previous state and system dynamics.
b. Covariance Estimation: Update the covariance matrix based on the system's dynamics and process noise.
***Step 3:* Update Based on Measurements:**
a. Kalman Gain Calculation: Compute the Kalman Gain using the predicted state and measurement noise covariance.
b. State Update: Adjust the state estimate using the Kalman Gain and the difference between the predicted and measured signals.
c. Covariance Update: Refine the covariance matrix using the Kalman Gain and measurement errors to enhance the estimate.
***Step 4:* Iteration:** Repeat the prediction and update steps iteratively for subsequent time steps, continually refining the state estimate based on new measurements.

C. FAULT DETECTION INDICES CALCULATION

Minimize downtime, maintain electrical network integrity, and allow for quick fault response with fault detection indices,

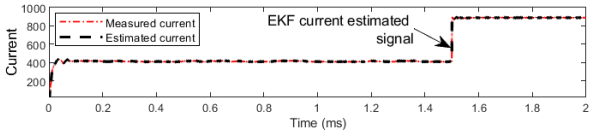

FIGURE 3. Comparision of the estimated and the measured current signal using EKF.

key decision-making tools. The occurrence of a fault in any DC line section of the MVDCDN causes transitory anomalies in current and voltage signals. Detecting these transient patterns reliably indicates the presence of a fault in any DC line section. Two indexes are computed in the proposed scheme for robust, reliable, and rapid responses to fault events.

i.) CR and,
ii.) DCDF

Both of these fault detection indexes are computed as follows:

i.) *CR index calculations*

The EKF predicts the expected measurement based on the current state estimate and the measurement model from eqs (4) (5), and (6):

$$\hat{i}_k\,(t) = H(\hat{x}_k, \emptyset_k) \tag{7}$$

where $\hat{i}_k\,(t)$ is the state estimate at time "t" represents any parameters, and $H(\,)$ is the measurement model function. The cumulative residual for the k^{th} sample of measurement is computed as the difference between the predicted and actual measurements:

$$CR_k\,(t) = \hat{i}_k\,(t) - i_k\,(t) \tag{8}$$

where is the $i_k\,(t)$ actual measurement at time "t". Moreover, the detailed steps involved in the computation of CR are as follows.

In first step, the residual covariance matrix $S_k\,(t)$ represents the uncertainty associated with the residual:

$$S_k\,(t) = H_k\,(t)\,P_k H_k^T + R_k\,(t) \tag{9}$$

where the $H_k\,(t)$ is the Jacobian matrix of the measurement model at time "t". P_k is the error covariance matrix of the state estimate at time "t". $R_k\,(t)$ is the measurement noise covariance matrix at time "t".

Then, the Kalman Gain $KG_k\,(t)$ determines the weight of the residual in updating the state estimate:

$$KG_k\,(t) = P_k(H_k^T)(S_k\,(t))^{-1} \tag{10}$$

In 2nd step, the state estimate $\hat{x}_k$ is corrected using the residual and Kalman Gain:

$$\hat{x}_k = \hat{x}_k + KG_k\,(t) * CR_k\,(t) \tag{11}$$

In 3rd step, update the error covariance matrix using the Kalman Gain and residual:

$$P_k = (I - KG_k\,(t)\,H_k)P_k \tag{12}$$

where "I "is the identity matrix. These steps represent the iterative process within the EKF, where the residuals are pivotal in refining the state estimate and improving the accuracy of the filtering process. The equations are repeatedly applied at each time step to update the state estimate based on new measurements.

Ultimately, the cumulative residual used for fault detection in the proposed technique is calculated and illustrated as shown below.

$$CR_k\,(t) = \hat{i}_k\,(t) - i_k\,(t) \tag{13}$$

ii.) *DCDF index calculations*

DCDF estimates the ratio or percentage of harmonic components of a DC signal relative to its fundamental component. It assesses distortion by examining higher-frequency components that differ from the ideal pure DC waveform. The DCDF formula is similar to the one used to calculate THD.

$$DCDF_k\,(t) = \frac{\sqrt{i_2\,(t)\,,\widehat{i_3(t)\,,i_5}\,(t)\,\ldots\ldots}}{i_1\,(t)} \times 100\% \tag{14}$$

The suggested protection technique identifies faults by monitoring changes in the CR, DCDF, or both indices. When the preset threshold value is exceeded, the scheme initiates the fault categorization and localization steps.

D. EKFBPE CALCULATION

To ensure the reliability and efficiency of network operation in the MVDCDN, the fault zone identification index plays a crucial role. Our presented strategy applies EKFBPE as the footing for fault classification and zone identification. By employing an extended Kalman filter, the EKFBPE computation examines the discrepancy between the anticipated and real conditions of the system. This analysis enables the algorithm to ascertain the degree of uncertainty or deviation in the prediction of EKFBPE. The proposed EKF technique utilizes the current signal to predict energy flow within the MVDCDN.

At first, the algorithm takes a look at the incoming current signal, which tells us about the power flow in the network. The EKF adjusts its estimation of the current as it goes along, taking into account both the dynamics of the system and any errors in the measurements. Using this calculation, the EKF makes predictions about how energy will flow in the MVDCDN in the future. As more data about the current signal comes in, these predictions keep getting updated, giving us a precise and up-to-the-minute estimate of energy flow.

In general, the EKFBPE algorithm functions as a reliable and effective method for estimating and predicting energy flow in the MVDCDN.

The calculation of EKFBPE involves integrating the current signal over time using the EKF. Now, let's delve into the steps involved in a detailed examination of the EKFBPE computation. In 1st step assume discrete time intervals "Δt" for numerical integration.

$$EKFBPE_k = E_{pridicted}\,(t_0) = 0 \tag{15}$$

For each time step t_i (where i ranges from 0 to n) obtain the current signal $I(t_i)$ at time t_i. In the second step, calculate the change in electrical energy during this interval using the trapezoidal rule for numerical integration:

$$\Delta E_k = \frac{1}{2}\left(I\left(t_i - 1\right) + I\left(t_i\right)\right) * \Delta t_k \tag{16}$$

It computes the area of the trapezoidal transformed of the current signal $I\left(t_i - 1\right)$ and $I\left(t_i\right)$ over the time interval "Δt". Next, in 3rd step, revise the predicted electrical energy by incorporating the deviation in energy:

$$E_{pridicted}\left(t_i\right) = E_{pridicted}\left(t_i - 1\right) + \Delta t_k \tag{17}$$

Proceed to the next time step and repeat the process until the final time point t_n is reached. Finally, the predicted electrical energy at the final time t_n is the accumulated sum obtained through the iterative process. The three-stage integration of eq (17) at $\hat{i}_k\left(t\right)$ results in the final mathematical relationship index used for fault classification and localization.

$$EKFBPE_k = \iiint \hat{i}_k\left(t\right)\left(t_i - 1\right)\Delta t_k \tag{18}$$

The numerical integration approach, using the trapezoidal rule, approximates the area under the curve of the current signal over discrete time intervals to estimate the predicted EKFBPE at each time step. Conclusively, the polarity of the EKFBPE, whether it is positive or negative, is then utilized for fault classification and localization decisions. This means that depending on the polarity, the algorithm can determine the type and location of the fault.

E. THRESHOLD CHOICE

The accuracy and effectiveness of any protection strategy heavily hinge upon the selection of threshold values. Inadequate threshold settings can result in failure to detect faults or may trigger operations during transient conditions. Consequently, in the proposed EKF-based strategy, extensive simulations under severe network conditions were conducted across multiple case studies. Firstly, a threshold constant value of 5 emerged as the optimal choice for current residuals, ensuring optimal performance and reliability. Secondly, the EKFBPE is opposite on both ends for Positive Pole to Ground faults, and negative on both ends for negative Pole to Ground faults, but for Pole-to-Pole faults EKFBPE is negative on one end while zero on another end.

IV. METHODOLOGY STEPS OF THE PROPOSED SCHEME

This section provides a step-by-step methodology of the proposed protection method. The outlined approach comprises five sequential steps. The initial step involves the measured current signal, while the second step is the initial processing of current and also emphasizes the state estimation of these signals using EKF. Subsequently, the Third step details the procedure for calculating fault detection indices named CR, DCDF. In the fourth step fault classification and localization index EKFBPE is discussed in detail. Finally, the fifth step elucidates the decision unit. A schematic diagram illustrating the EKF-based strategy is presented to offer a visual representation of the methodology in **FIGURE 4.**

A. MEASURMENT UNIT

Measurement for any relay unit is a fundamental aspect of ensuring the reliable and correct tripping decision. Proposed protection relays use current transformers (CTs) to measure electrical currents flowing through DC distribution lines in the adapted MVDCDN. Initially, the DC current signal measured from the respective faulty bus contains inherent measurement noise and incidental errors. These current signals are analog by nature while the proposed algorithm needs discreate data to process for accurate and precise decision.

B. INITIAL-PROCESSING UNIT

Then, two tasks are performed by this unit. Firstly, the measured analog signals undergo conversion to digital format using a 12-bit analog-to-digital converter operating at a sampling frequency of 3.6 kHz. Subsequently, the converted current signal is subjected to processing through a second-order low-pass Bessel filter with a cut-off frequency of 1600 Hz. The primary aim of employing the Butterworth filter is to mitigate aliasing effects in the signals. Secondly, the discrete current signal obtained is fed into the Extended Kalman Filter. The EKF undertakes two key tasks: (i). Filtering out noise within the acquired current signal, whether it's measurement noise or arbitrary noise. (ii). Estimating the features within the discrete current signal on a sample-by-sample basis. The estimated discrete DC current signals are then provided to the next stage for index generation.

C. FAULT DETECTION INDEX GENERATION UNIT

In any protection method, the fault detection unit is very crucial for successful operation by avoiding false tripping and blinding issues. In the proposed scheme the current signal is used for generation of robust fault detection indexes. After successful state estimation of the measured current signal, fault detection indexes are generated. The CR is generated through eq (13) by subtracting measured discrete current from estimated/filtered EKF. The detailed step by step calculation of EKF based CR is mentioned in eq (7) to (13). These steps represent the iterative process within the EKF, where the residual is pivotal in refining the state estimate and improving the accuracy of the filtering process. The equations are repeatedly applied at each time step to update the state estimate based on new measurements to generate CR. Secondly, another index named DCDF is computed using eq (14). It is just similar to conventional total harmonic distortion. If the value of CR & DCDF is more than 5 constant threshold value, it enables the fault classification and zone identification unit.

D. FAULT CLASSIFICATION AND ZONE IDENTIFICATION

After there, when a fault is successfully detected then the fault classification and zone identification unit start its operation

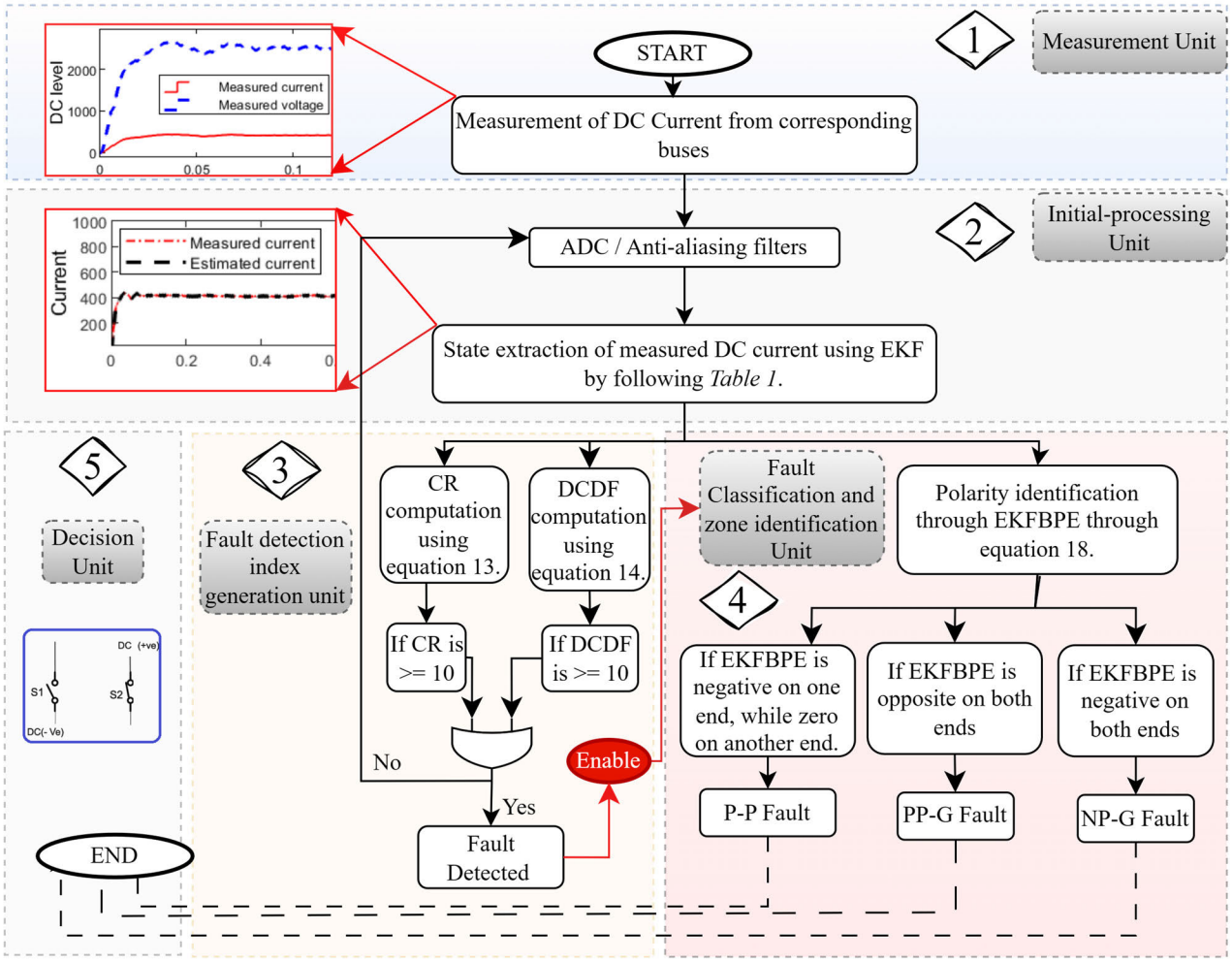

FIGURE 4. Schematic diagram of the proposed protection scheme.

in two stages. In the 1st stage the polarity of EKFBPE is identified. Then, in the 2nd stage the relays positioned at both ends of a faulty pole register the polarities and communicate with their corresponding relays. The EKFBPE for a PP-G fault on any DC Line Section, relays on the corresponding pole (either positive or negative) exhibit opposite polarities, while those on the NP-G pole display negative polarities on both ends. Conversely, in a pole-to-pole fault scenario on any section similar polarities on both ends or no change in any one end.

E. DECISION UNIT

Ultimately, once the determination is made regarding which fault has occurred within the MVDCDN in which section, this information is transmitted to the tripping circuitry. This transmission prompts the tripping circuitry to take action, specifically activating the relevant circuit breaker (CB) in the section of the network affected by the fault. This deliberate action aims to isolate and clear the fault, ensuring the overall stability and safety of the MVDCDN.

V. SIMULATION RESULTS

This section focusses on the simulation results examining of several DC fault situations that were simulated within the MVDCDN test bed. The tested simulations of faults are categorized into three types: positive pole to ground (PP-G), negative pole to ground (NP-G), and pole to pole (P-P) under radial, looped and meshed conditions. Moreover, No-fault and transient conditions were also tested. Effect of resistance and scheme effect on voltage is also examined. Hence, through extensive simulation it is examined that proposed scheme performed well.

A. POSITIVE POLE TO GROUND

A PP-G fault in an MVDCDN happens once the positive conductor/pole of the DC line comes into contact with the grounding. This failure scenario can cause serious problems inside the MVDCDN and requires immediate response to guarantee system safety and stability. Therefore, several PP-G faults were simulated in different test conditions to validate the performance of the proposed method.

Several PP-G faults results of different scenarios are mentioned in TABLE 2. However, due to space constraints and for reader convenience, a singular case study is visualized here as an example. A PP-G fault hit the DC line section 14 at 2o km away from relay 777 at a time instant of 0.1 ms. The relay 777 reads the current measurements, CR, and DCDF as depicted in **FIGURE 5**. It is shown that the CR and DCDF are more than the predefined threshold level at the fault inception time stamp. It illustrates that the corresponding PP-G fault is successfully detected by the proposed method. Moreover, the opposite polarity on both Relay 777 and Relay 888 indicates that the PP-G fault occurred in DC line section 14.

B. NEGATIVE POLE TO GROUND

A negative pole-to-ground fault in an MVDCDN occurs when the negative conductor or pole of the DC network comes into contact with the grounding or earth reference. NP-G faults are very challenging to detect because of low fault current magnitude, and lack of zero crossing. Hence, multiple NP-G faults were simulated across various test conditions to assess and confirm the effectiveness of the proposed methodology or approach.

Several NP-G faults results of different scenarios are mentioned in TABLE 2. However, due to space constraints and for reader convenience, a singular case study is visualized here as an example. An NP-G fault occurred at DC line section 18 5 km away from relay 515 at a time instant of 0.1 ms. The relay 515 reads the current measurements, CR, and DCDF as depicted in **FIGURE 6**. It is shown that the CR fails to detect the corresponding fault while the DCDF is more than the predefined threshold level at fault inception time. It illustrates that the corresponding NP-G fault is successfully detected by the dual index of the proposed method. Moreover, the similar polarity on both Relay 515 and Relay 616 indicates that the NP-G fault occurred in DC line section 18.

C. POLE TO POLE

Pole-to-pole faults in an MVDCDN occur when there's a direct short circuit between the positive and negative poles or conductors of the DC network. Consequently, numerous simulations of pole-to-pole faults were conducted under diverse test conditions to evaluate and validate the efficiency of the proposed methodology.

Several P-P faults results of different scenarios are mentioned in TABLE 2. However, due to space limitations and for the reader's convenience, a single case study is presented here as an illustrative example. A P-P fault hit the DC line section 15 at 10 km away from relay 999 at a time instant of 0.2 ms. Relay 999 reads the current measurements, CR, and DCDF as depicted in **FIGURE 7**. It is shown that the CR is more than the predefined threshold level at the fault inception time stamp. However, DCDF fails to detect P-P fault conditions. Conclusively, it is illustrated that the corresponding P-P fault is successfully detected by the proposed method because of the novel dual index. Moreover, the polarity on Relay 999 is negative while the polarity on Relay 000 is zero/ no change. Hence, it indicates that the P-P fault occurred in DC line section 15.

D. EFFECT OF FAULT RESISTANCE

The impact of fault resistance is crucial for designing effective protective schemes, ensuring system reliability, and minimizing the potential risks associated with fault conditions. Protective devices and system designs must account for varying fault resistances to effectively detect and mitigate faults while maintaining the stability and safety of the MVDCDN. Subsequently, various simulations involving faults characterized by different resistance values were executed across a range of test scenarios to assess and affirm the effectiveness of the proposed methodology.

Several fault scenarios with different resistances are mentioned in TABLE 3. Conclusively, it is observed from detailed fault analysis on different resistances, that more than a 50-ohm scheme fails to detect faults. As mentioned in TABLE 3 the fault scenarios whose resistance is more than 50 ohm their fault detection and classification indices are zero. However, in consideration of space constraints and to ensure reader accessibility, a singular case study is visualized here as an illustrative example. A P-P fault hit the DC line section 11 at 13 km away from relay 111 at a time instant of 0.25 ms. CR and DCDF computed at Relay 111 are depicted in **FIGURE 8**. It is shown that the CR and DCDF up to the resistance value of 48 ohms is more than the predefined threshold level at fault inception time stamp 0.25.

To validate the performance and robustness of proposed method during high impedance faults. Therefore, we had included a case study with the resistance 50 ohm. An NP-G fault occurred at DC line section 11, 35 km away from relay 111 at a time instant of 0.25 ms. The relay 111 reads the current measurements, CR, and DCDF as depicted in **FIGURE 9**. It is shown that the CR fails to detect the corresponding fault while the DCDF is more than the predefined threshold level at fault inception time. It illustrates that the corresponding NP-G fault at 50 ohms is successfully detected by the dual index of the proposed method. Moreover, the similar polarity on both Relay 111 and Relay 222 indicates that the NP-G fault occurred in DC line section 11.

E. MESHED MVDCDN TOPOLOGY CASE STUDY

In this section, we present the results of case studies conducted on looped and meshed medium voltage DC distribution systems. These cases aim to assess the performance and reliability of these systems under various topological structures. Simulations on several such cases were performed but due to space limitations and ease of readers understanding only one such case is presented here.

A PP-G fault occurred at DC line section 16, 15 km away from relay 121 at a time instant of 0.15 ms. Moreover, the Switch-1 and switch-2 are closed to generate looped and meshed topology. The relay 121 reads the current measurements, CR, and DCDF as depicted in **FIGURE 10**. It is shown that the during meshed topology both the CR and

TABLE 2. Multiple DC faults at various conditions and locations in MVDCDN.

Faulty section	Fault types	Fault location	Fault detection indexes		EKFBPE (polarity)
			CR (peak)	DCDF (peak)	
DC Line section 11	PP-G	20 km from B0	25	36	+ive Relay 111 while -ive at Relay 222
DC Line section 12	NP-G	10 km from B1	0	50	-ive Relay 333 while -ive at Relay 444
DC Line section 13	P-P	05km from B0	55	0	-ive Relay 555 while zero at Relay 666
DC Line section 14	PP-G	15km from B2	39	45	+ive Relay 777 while -ive at Relay 888
DC Line section 15	NP-G	25km from B0	0	90	-ive Relay 999 while -ive at Relay 000
DC Line section 16	P-P	13km from B3	68	0	-ive Relay 121 while zero at Relay 212
DC Line section 17	NP-G	17km from B0	0	73	-ive Relay 313 while -ive at Relay 414
DC Line section 18	PP-G	28km from B4	60	97	+ive Relay 515 while -ive at Relay 616

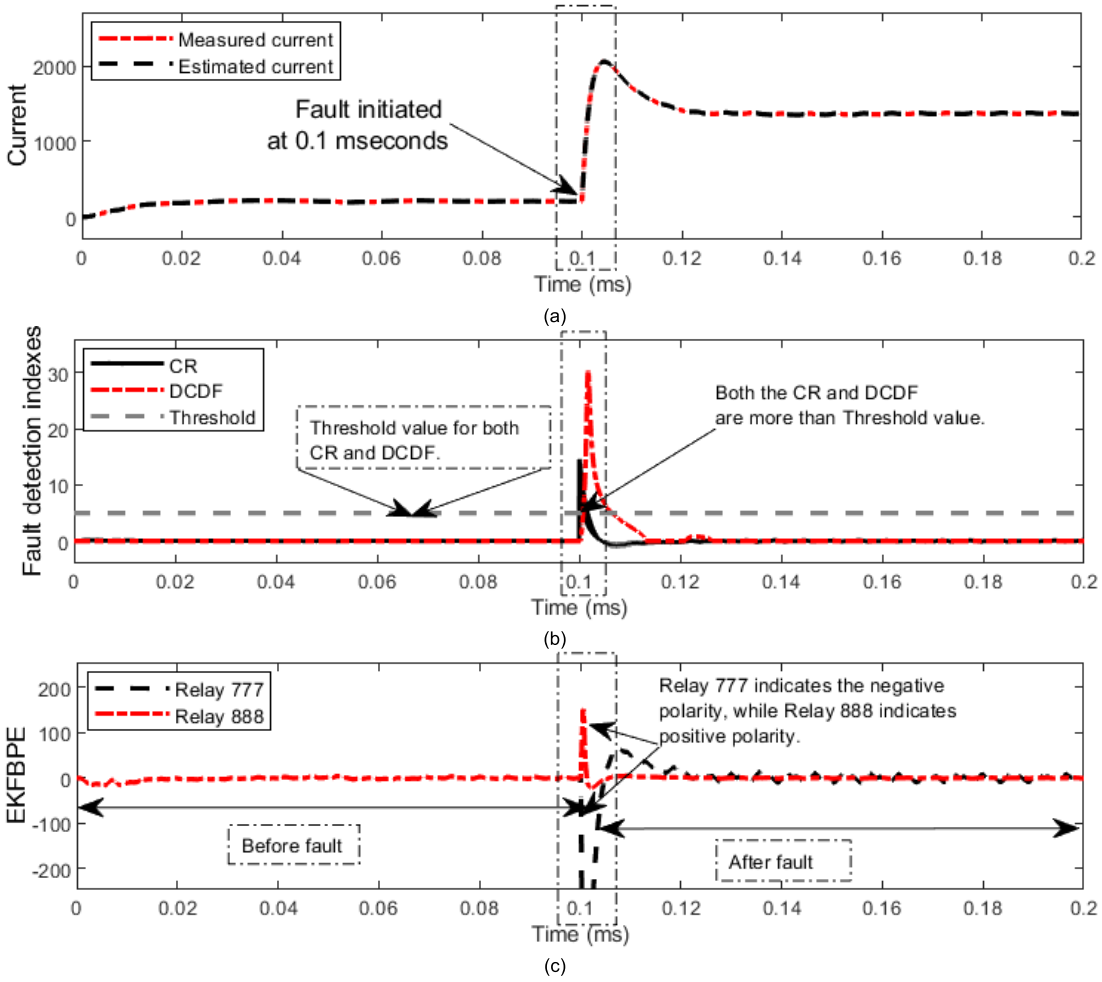

FIGURE 5. PP-G fault at 0.1 ms in DC line section 14. (a) current signature measured/estimated. (b) fault detection indexes CR & DCDF. (c) EKFBPE polarity signature.

DCDF are more than the predefined threshold level at fault inception time. It illustrates that the corresponding PP-G fault is successfully detected by the dual index of the proposed method during meshed and looped condition. Moreover, the opposite polarity on both Relay 121 and Relay 212 indicates that the PP-G fault occurred in DC line section 16.

F. NO FAULT/TRANSIENT CASE STUDY

In order to illustrate the concept of no-fault or transient cases, several cases were simulated but due to space constraint a singular case study is presented here.

An AC load switching on bus 5 occurs at 0.3 ms to generate a transient/ switching condition. The relay 444 reads

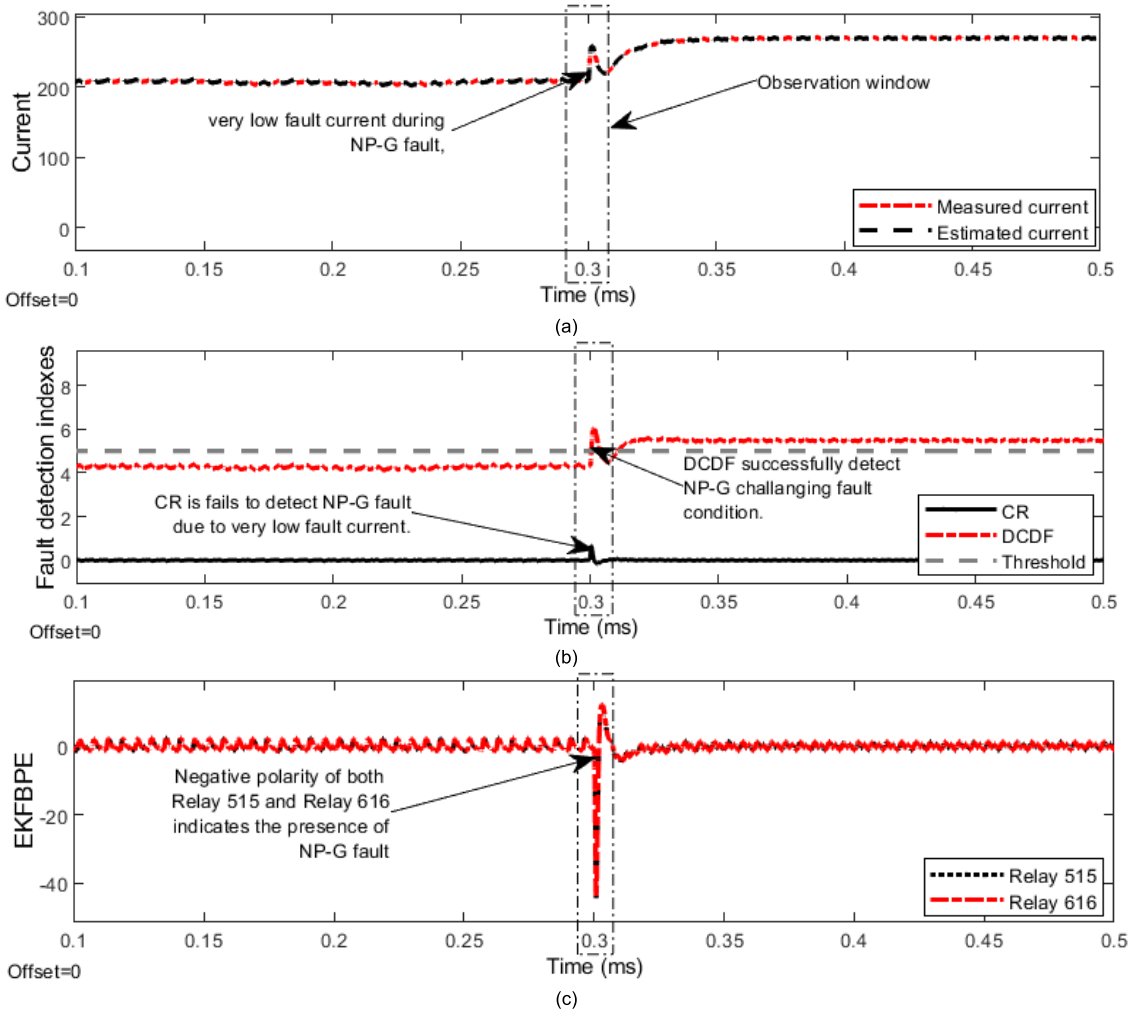

FIGURE 6. NP-G fault at 0.3 ms in DC line section 18. (a) current signature mesured/estimated. (b) fault detection indexes CR & DCDF. (c) EKFBPE polarity signature.

TABLE 3. Multiple DC faults at various resistances in the MVDCDN.

Faulty section	Fault types	Fault Resistance	Fault detection indexes		Fault Location
			CR (peak)	DCDF (peak)	
DC Line section 11	NP-G	0.1 ohms	0	46	25 km from B0
DC Line section 12	P-P	05 ohms	55	0	15 km from B1
DC Line section 13	NP-P	10 ohms	0	80	12 km from B0
DC Line section 14	PP-G	20 ohms	19	85	15 km from B2
DC Line section 15	P-P	10 ohms	50	0	20 km from B0
DC Line section 16	NP-P	50 ohms	0	80	12 km from B3
DC Line section 17	NP-G	75 ohms	0	0	16 km from B0
DC Line section 18	PP-G	100 ohms	0	0	22 km from B4

the current measurements, CR, and DCDF as depicted in **FIGURE 11**. It is shown that during the transient/ switching event both the CR and DCDF are less than the predefined threshold level. It indicates that the proposed scheme does not maloperation during no-fault transient/ switching condition and successfully operate.

G. TIME OF ACTION AND SCHEME EFFECT ON VOLTAGE CASES

In analyzing the impact of the protection scheme operation on voltage stability, it is crucial to consider the time of action of the scheme in response to various fault scenarios. The effectiveness of the protection scheme in mitigating

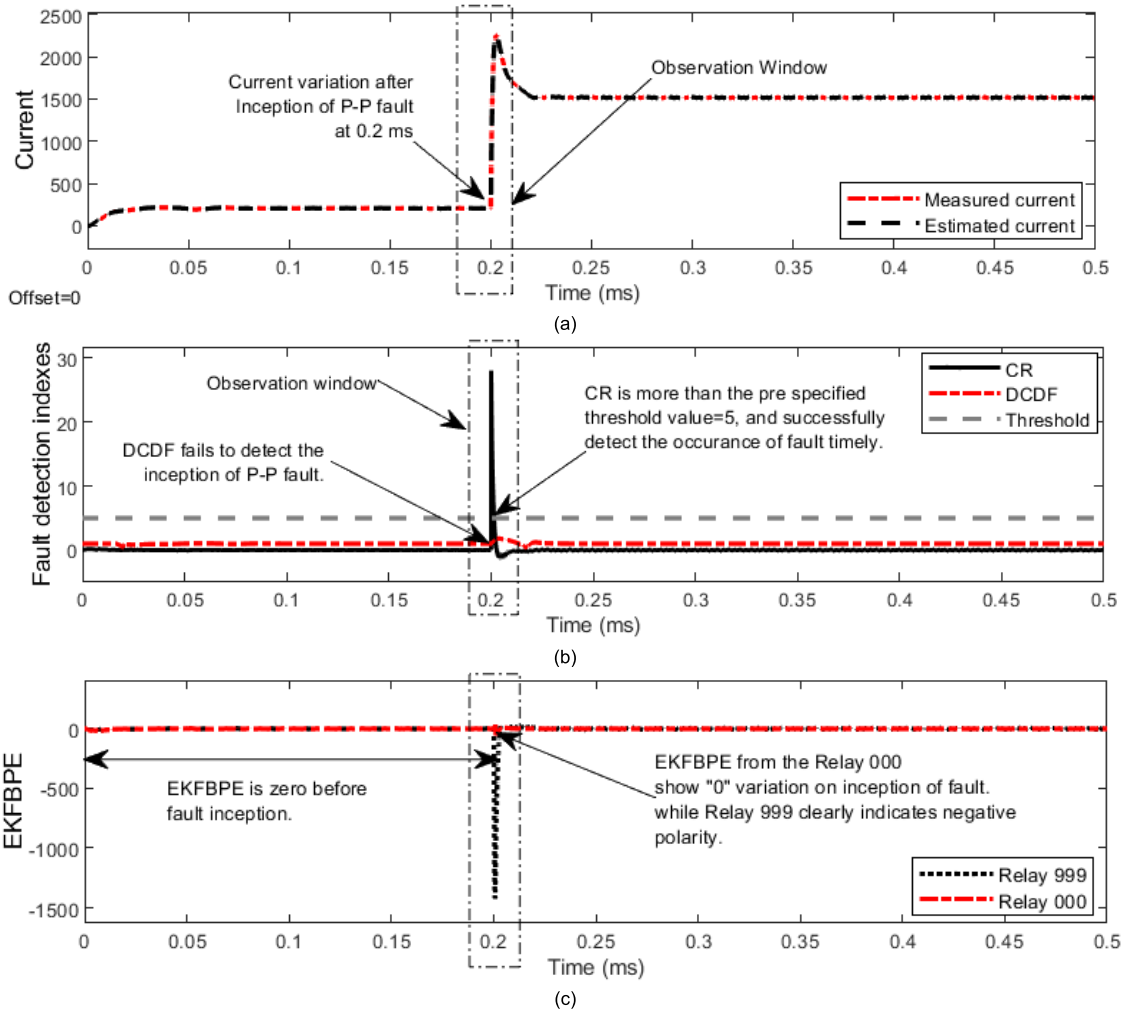

FIGURE 7. P-P fault at 0.2 ms in DC line section 15. (a) current signature measured/estimated. (b) fault detection indexes CR & DCDF. (c) EKFBPE polarity signature.

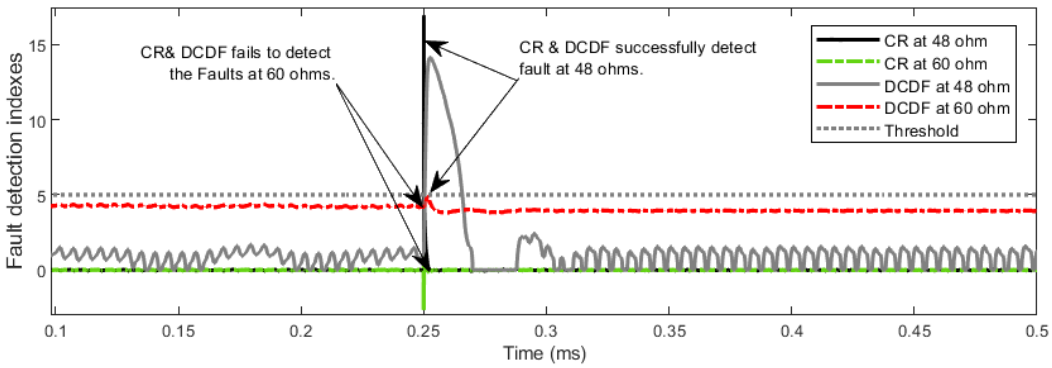

FIGURE 8. Fault detection indexes CR & DCDF of fault resistance effect on proposed scheme case simulation at DC line section 11.

voltage fluctuations depends on how quickly it detects and responds to faults within the MVDCDN. Through comprehensive voltage analysis, the scheme's performance can be assessed, enabling improvements to be made to enhance grid resilience and optimize operational efficiency. Several cases are simulated but due to space constraint on such case is presented here to depict the performance of proposed scheme.

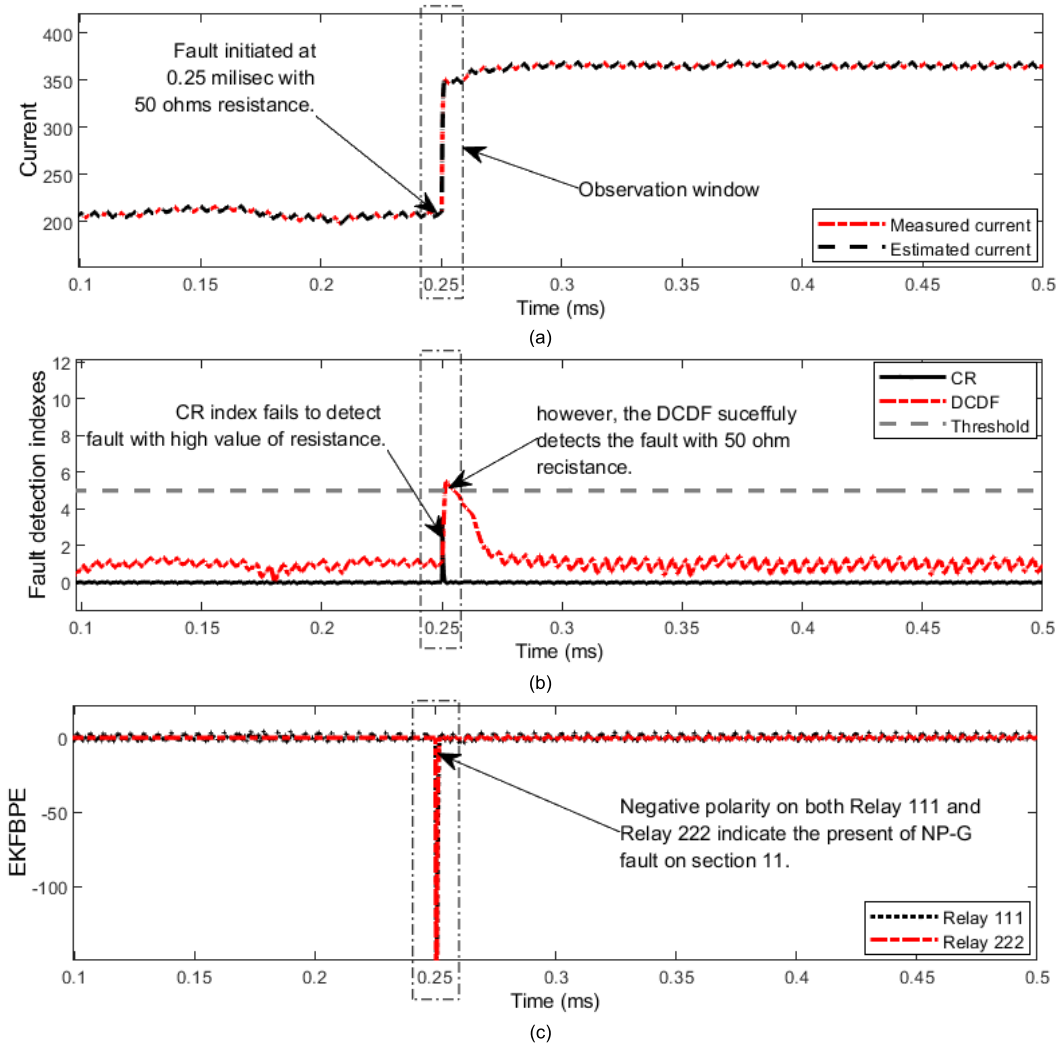

FIGURE 9. NP-G fault at 0.25 ms in DC line section 11. (a) current signature mesured/estimated. (b) fault detection indexes CR & DCDF. (c) EKFBPE polarity signature.

TABLE 4. Comparitive analysis of proposed scheme with excisting benchmark schemes.

Comparison Parameters	Compared benchmark Methods				Proposed scheme
	Mathematical morphology-based scheme.	Pseudo-data-driven-based scheme.	ANN-based scheme.	Entropy-based scheme.	
Time of action	<5msec	75 sec	3msec	1msec	1 msec
Computational latency	Low	Very High	High	High	Very low
Accuracy (%)	95.5%	97.5%	99.38%	100%	99.9%
Topological structure	Only radial	Only meshed	Only meshed	Only radial and looped	All Topological structure
Resilience to different faults	✓	×	×	✓	✓
Noise Consideration	×	✓	✓	×	✓

A P-P fault occurred at DC line section 13, 45 km away from relay 555 at a time instant of 0.25 ms. Moreover, the Switch-1 is open, and the switch-2 is closed to generate looped topology. Relay 555 reads the current measurements, voltage measurements, as depicted in **FIGURE 12**. It is shown that the fault is cleared swiftly by the proposed scheme

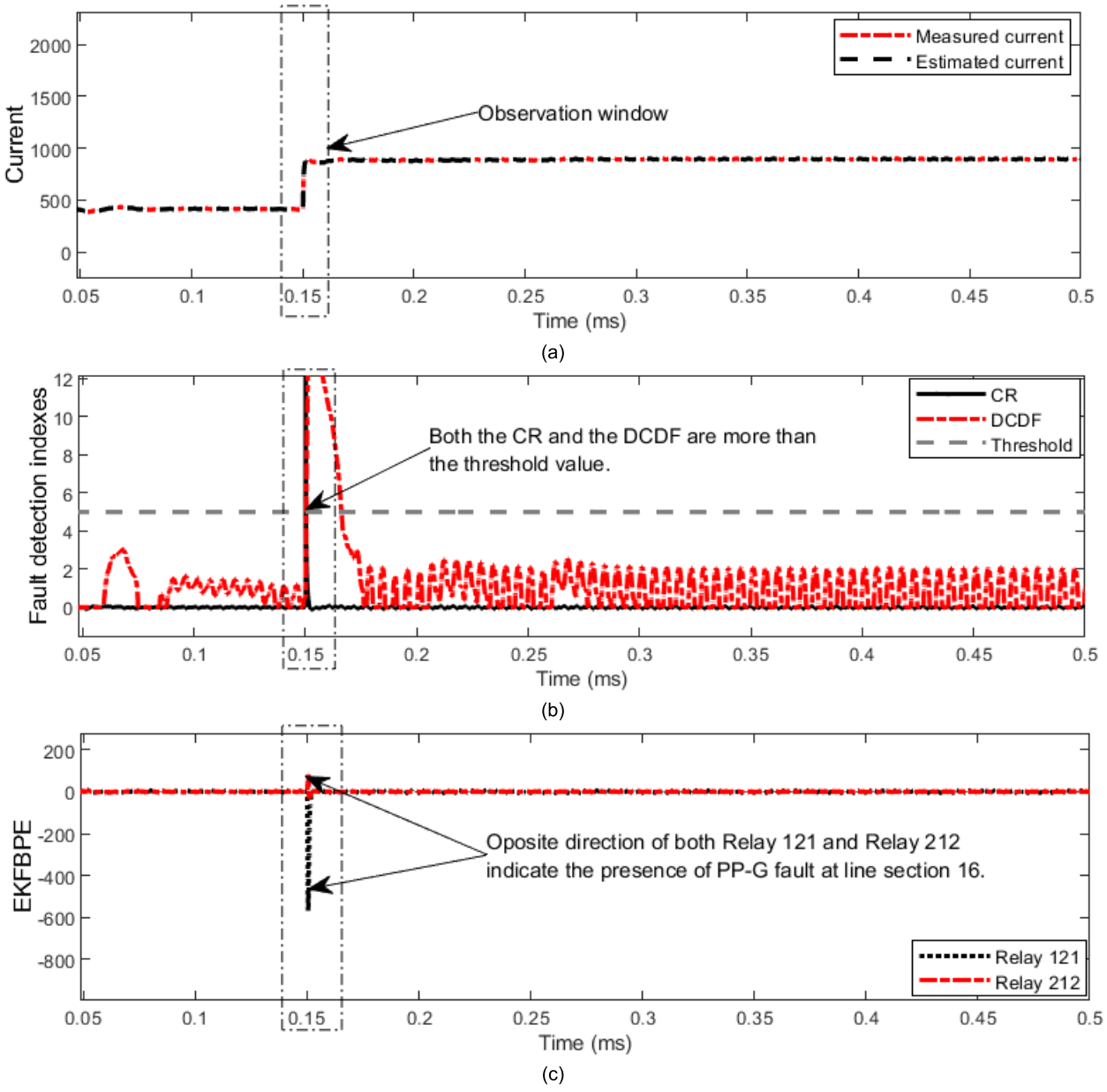

FIGURE 10. PP-G fault at 0.15 ms in DC line section 16. (a) current signature mesured/estimated. (b) fault detection indexes CR & DCDF. (c) EKFBPE polarity signature.

in less than 1 ms. The voltage sag appears during the fault condition, but the voltage is restored after the successful operation of Relay 555.

Hence, it's proved that the scheme detects, classify, and locate the faults successfully in less than 1 msec, additionally 4 cycle is needed by CB for tripping.

VI. COMPARATIVE ANALYSIS

In comparison to the existing benchmark schemes including Mathematical morphology-based scheme [9], Pseudo-data-driven-based scheme [22], ANN-based scheme [29], and Entropy-based scheme [18]. It is shown in TABLE 4 that the proposed scheme demonstrates significant improvements in accuracy, computational burden, and operation time. The accuracy of the proposed scheme outperforms the benchmark method through its advanced algorithms and enhanced data processing techniques. Additionally, the computational burden is significantly reduced in the proposed scheme due to the implementation of efficient algorithms that optimize resource utilization. This reduction in computational burden not only improves system performance but also enhances scalability for handling larger datasets. Moreover, the operation time is greatly reduced in the new scheme as it leverages state-of-the-art technologies, allowing for faster data processing and decision-making. Moreover, the proposed scheme shows resilience to different kind of DC faults, during its

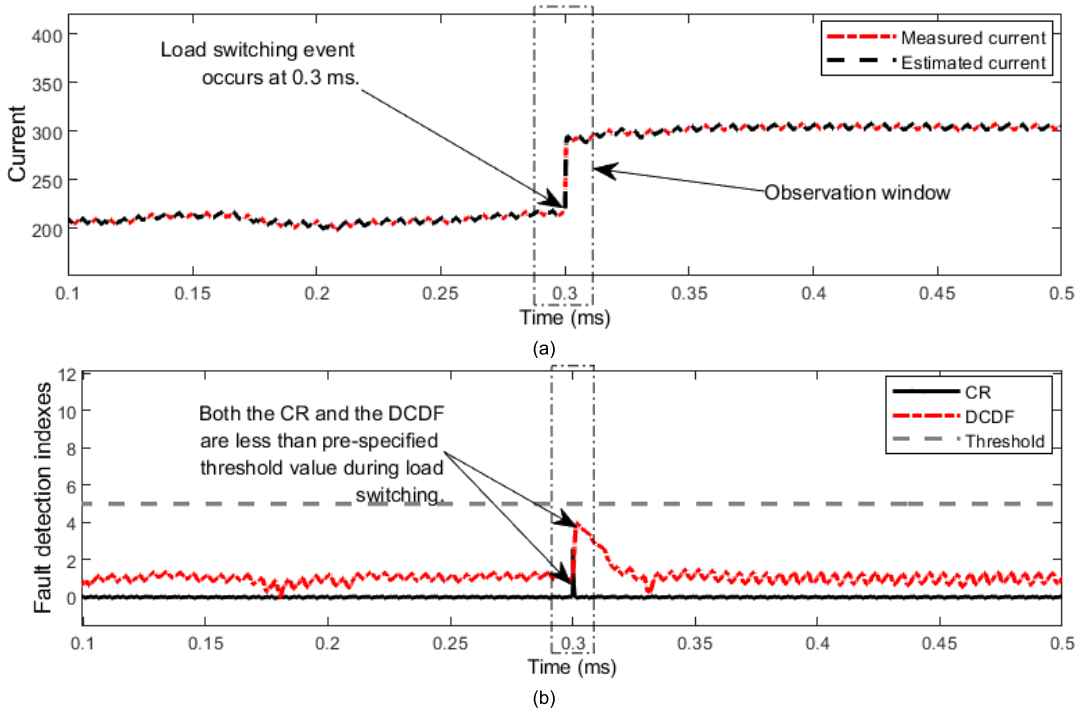

FIGURE 11. Load switching event at 0.3 ms in DC line section 12. (a) current signature mesured/estimated. (b) fault detection indexes CR & DCDF.

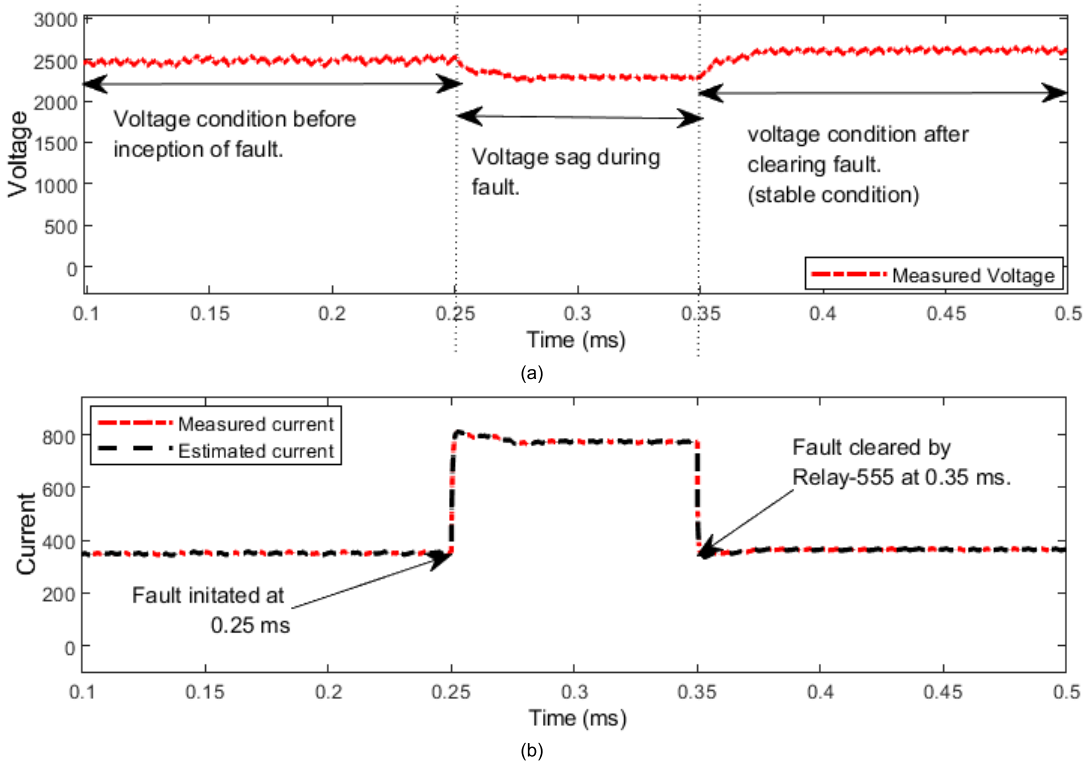

FIGURE 12. Time of action, and voltage stability anlysis.

operation in radial, looped and meshed network topology. It's the additional feature of the scheme that it deals with noisy measurements. Overall, the proposed scheme surpasses the existing benchmark method in terms of accuracy,

computational burden, and operation time, providing a more efficient and effective solution for the intended application.

VII. CONCLUSION

This paper presented an innovative approach utilizing the Extended Kalman filter to detect diverse DC faults exclusively from current signals in the MVDCDN. Initially, current signals from corresponding positive and negative poles were processed by the EKF, generating cumulative residuals and DC distortion factor as fault detection indices. Activation of the fault classification/zone identification unit was triggered by changes detected in CR and DCDF within the relay's observation window. Subsequently, the FCZI unit computed Extended Kalman filter-based predicted energy for faulted DC line sections, enabling fault classification and localization. This protection strategy necessitated low-band wireless communication within the smart grid. Through extensive simulations on a ±2.5 kV MVDCDN with three feeders utilizing MATLAB® Simulink 2022b, the proposed scheme demonstrated 99.9% accuracy, swift operation under radial, looped, and meshed topology, and robust resilience against various fault types.

REFERENCES

[1] S. Mohanty, A. Bhanja, S. P. Gautam, D. Chittathuru, S. K. Dash, M. Mangaraj, R. Chinthaginjala, and A. M. Alamri, "Review of a comprehensive analysis of planning, functionality, control, and protection for direct current microgrids," *Sustainability*, vol. 15, no. 21, p. 15405, Oct. 2023, doi: 10.3390/su152115405.

[2] S. S. Rangarajan, R. Raman, A. Singh, C. K. Shiva, R. Kumar, P. K. Sadhu, E. R. Collins, and T. Senjyu, "DC microgrids: A propitious smart grid paradigm for smart cities," *Smart Cities*, vol. 6, no. 4, pp. 1690–1718, Jul. 2023, doi: 10.3390/smartcities6040079.

[3] K. Kant and O. H. Gupta, "DC microgrid: A comprehensive review on protection challenges and schemes," *IETE Tech. Rev.*, vol. 40, no. 4, pp. 574–590, Jul. 2023, doi: 10.1080/02564602.2022.2136271.

[4] L. Tang, Y. Han, A. S. Zalhaf, S. Zhou, P. Yang, C. Wang, and T. Huang, "Resilience enhancement of active distribution networks under extreme disaster scenarios: A comprehensive overview of fault location strategies," *Renew. Sustain. Energy Rev.*, vol. 189, Jan. 2024, Art. no. 113898, doi: 10.1016/j.rser.2023.113898.

[5] S. A. Hosseini, B. Taheri, S. H. H. Sadeghi, and A. Nasiri, "An overview of DC microgrid protection schemes and the factors involved," *Electr. Power Compon. Syst.*, vol. 2023, pp. 1–31, Sep. 2023, doi: 10.1080/15325008.2023.2251469.

[6] M. S. Alam, F. S. Al-Ismail, S. M. Rahman, M. Shafiullah, and M. A. Hossain, "Planning and protection of DC microgrid: A critical review on recent developments," *Eng. Sci. Technol., Int. J.*, vol. 41, May 2023, Art. no. 101404, doi: 10.1016/j.jestch.2023.101404.

[7] F. Mumtaz, K. Imran, A. Abusorrah, and S. B. A. Bukhari, "Harmonic content-based protection method for microgrids via 1-dimensional recursive median filtering algorithm," *Sustainability*, vol. 15, no. 1, p. 164, Dec. 2022, doi: 10.3390/su15010164.

[8] Q. Wan, S. Zheng, and C. Shi, "A rapid diagnosis technology of short circuit fault in DC microgrid," *Int. J. Electr. Power Energy Syst.*, vol. 147, May 2023, Art. no. 108878, doi: 10.1016/j.ijepes.2022.108878.

[9] M. A. Shah, S. B. A. Bukhari, K. Imran, K. K. Mehmood, F. Mumtaz, A. Abusorrah, S. A. A. Kazmi, and A. Wadood, "High speed protection of medium voltage DC distribution system using modified mathematical morphology," *IET Renew. Power Gener.*, vol. 16, no. 14, pp. 3134–3148, Oct. 2022, doi: 10.1049/rpg2.12564.

[10] N. Bayati, H. R. Baghaee, A. Hajizadeh, M. Soltani, and Z. Lin, "Mathematical morphology-based local fault detection in DC microgrid clusters," *Electr. Power Syst. Res.*, vol. 192, Mar. 2021, Art. no. 106981, doi: 10.1016/j.epsr.2020.106981.

[11] K. Saleh, A. Hooshyar, and E. F. El-Saadany, "Fault detection and location in medium-voltage DC microgrids using travelling-wave reflections," *IET Renew. Power Gener.*, vol. 14, no. 4, pp. 571–579, Mar. 2020, doi: 10.1049/iet-rpg.2019.0370.

[12] D. Wang, M. Hou, M. Gao, and F. Qiao, "Travelling wave directional pilot protection for hybrid LCC-MMC-HVDC transmission line," *Int. J. Electr. Power Energy Syst.*, vol. 115, Feb. 2020, Art. no. 105431, doi: 10.1016/j.ijepes.2019.105431.

[13] A. Sistani, S. A. Hosseini, V. S. Sadeghi, and B. Taheri, "Fault detection in a single-bus DC microgrid connected to EV/PV systems and hybrid energy storage using the DMD-IF method," *Sustainability*, vol. 15, no. 23, p. 16269, Nov. 2023, doi: 10.3390/su152316269.

[14] B. Taheri and A. Shahhoseini, "Direct current (DC) microgrid control in the presence of electrical vehicle/photovoltaic (EV/PV) systems and hybrid energy storage systems: A case study of grounding and protection issue," *IET Gener., Transmiss. Distrib.*, vol. 17, no. 13, pp. 3084–3099, Jul. 2023, doi: 10.1049/gtd2.12882.

[15] G. K. Rao and P. Jena, "A novel fault identification and localization scheme for bipolar DC microgrid," *IEEE Trans. Ind. Informat.*, vol. 19, no. 12, pp. 11752–11764, Dec. 2023, doi: 10.1109/TII.2023.3252409.

[16] A. M. Aboelezz, A. A. Eladl, M. T. Abo Amasha, M. H. Elderigi, M. A. Mohamed, S. W. Aldoadoa, A. R. Elhamedy, H. M. Alnegeri, T. M. Elshreef, A. A. Eldwany, M. S. Shabka, B. N. Alhasnawi, B. E. Sedhom, and V. Bureš, "Efficient fault detection, localization, and isolation in MT-HVDC systems based on distance protection and LoRaWAN communication," *Energy Rep.*, vol. 10, pp. 4183–4197, Nov. 2023, doi: 10.1016/j.egyr.2023.10.083.

[17] N. R. Nareddy, R. Pitchaimuthu, and M. Sridharan, "Current index based protection technique for low voltage DC microgrid," *Electr. Power Syst. Res.*, vol. 220, Jul. 2023, Art. no. 109360, doi: 10.1016/j.epsr.2023.109360.

[18] R. Rahmani, S. H. H. Sadeghi, H. Askarian-Abyaneh, and M. J. Emadi, "An entropy-based scheme for protection of DC microgrids," *Electr. Power Syst. Res.*, vol. 228, Mar. 2024, Art. no. 110010, doi: 10.1016/j.epsr.2023.110010.

[19] F. Mumtaz, H. H. Khan, A. Zafar, M. U. Ali, and K. Imran, "A state-observer-based protection scheme for AC microgrids with recurrent neural network assistance," *Energies*, vol. 15, no. 22, p. 8512, Nov. 2022, doi: 10.3390/en15228512.

[20] M. Y. Arafat, M. J. Hossain, and M. M. Alam, "Machine learning scopes on microgrid predictive maintenance: Potential frameworks, challenges, and prospects," *Renew. Sustain. Energy Rev.*, vol. 190, Feb. 2024, Art. no. 114088, doi: 10.1016/j.rser.2023.114088.

[21] R. Montoya, B. P. Poudel, A. Bidram, and M. J. Reno, "DC microgrid fault detection using multiresolution analysis of traveling waves," *Int. J. Electr. Power Energy Syst.*, vol. 135, Feb. 2022, Art. no. 107590, doi: 10.1016/j.ijepes.2021.107590.

[22] W. Javed, D. Chen, and I. Kucukdemiral, "Fault identifiability and pseudo-data-driven fault localization in a DC microgrid," *Int. J. Electr. Power Energy Syst.*, vol. 148, Jun. 2023, Art. no. 108944, doi: 10.1016/j.ijepes.2023.108944.

[23] S. Veerapandiyan and V. Sugavanam, "On-line fault identification, location, and seamless service restoration using transfer learning-based convolution neural network for low-voltage DC microgrid," *Electr. Power Compon. Syst.*, vol. 51, no. 8, pp. 785–808, May 2023, doi: 10.1080/15325008.2023.2183997.

[24] D. K. J. S. Jayamaha, N. W. A. Lidula, and A. D. Rajapakse, "Wavelet-multi resolution analysis based ANN architecture for fault detection and localization in DC microgrids," *IEEE Access*, vol. 7, pp. 145371–145384, 2019, doi: 10.1109/ACCESS.2019.2945397.

[25] Y. Ma, A. Maqsood, D. Oslebo, and K. Corzine, "Wavelet transform data-driven machine learning-based real-time fault detection for naval DC pulsating loads," *IEEE Trans. Transport. Electrific.*, vol. 8, no. 2, pp. 1956–1965, Jun. 2022, doi: 10.1109/TTE.2021.3130044.

[26] F. Mumtaz, K. Imran, H. Rehman, and H. A. Qureshi, "Hardware supported fault detection and localization method for AC microgrids using mathematical morphology with state observer algorithm," *IEEE Access*, vol. 12, pp. 12446–12457, 2024, doi: 10.1109/ACCESS.2024.3354790.

[27] F. Mumtaz, K. Imran, S. B. A. Bukhari, K. K. Mehmood, A. Abusorrah, M. A. Shah, and S. A. A. Kazmi, "A Kalman filter-based protection strategy for microgrids," *IEEE Access*, vol. 10, pp. 73243–73256, 2022, doi: 10.1109/ACCESS.2022.3190078.

[28] D. Efimov, A. Zolghadri, and P. Simon, "Improving fault detection abilities of extended Kalman filters by covariance matrices adjustment," in *Proc. Conf. Control Fault-Tolerant Syst. (SysTol)*, Oct. 2010, pp. 131–136, doi: 10.1109/SYSTOL.2010.5676002.
[29] M. Z. Yousaf, S. Khalid, M. F. Tahir, A. Tzes, and A. Raza, "A novel DC fault protection scheme based on intelligent network for meshed DC grids," *Int. J. Electr. Power Energy Syst.*, vol. 154, Dec. 2023, Art. no. 109423, doi: 10.1016/j.ijepes.2023.109423.

NAUMAN ALI LARIK received the B.Eng. degree in electrical engineering from QUEST Nawabshah, Pakistan, in 2011, and the M.S. degree in electrical engineering from Xi'an Jiaotong University, Xi'an, Shaanxi, China, in 2015. He is currently pursuing the Ph.D. degree with the School of Electric Power Engineering, South China University of Technology, Guangzhou, China. He was a Lecturer for two years with DHA Suffa University, Pakistan.

MENG SHI LI received the M.Sc. (Eng.) degree (Hons.) in information and intelligence engineering from the Department of Electrical Engineering and Electronics, The University of Liverpool, U.K., in 2005, and the Ph.D. degree in electrical engineering from The University of Liverpool, in 2010. He is currently an Associate Professor with the School of Electric Power, South China University of Technology. His research interests include computational intelligence and their applications in power systems.

QING HUA WU received the M.Sc. (Eng.) degree in electrical engineering from Huazhong University of Science and Technology, Wuhan, China, in 1981, and the Ph.D. degree in electrical engineering from Queen's University Belfast (QUB), Belfast, U.K., in 1987. From 1981 to 1984, he was a Lecturer with the Department of Electrical Engineering, Huazhong University of Science and Technology. He was a Research Fellow and subsequently a Senior Research Fellow with QUB, from 1987 to 1991. He was a Lecturer with the Department of Mathematical Sciences, Loughborough University, Loughborough, U.K., in 1991. He was appointed as a Senior Lecturer. In September 1995, he joined The University of Liverpool, Liverpool, U.K., to take up his appointment to the Chair of electrical engineering with the Department of Electrical Engineering and Electronics. He is currently a Distinguished Professor with the School of Electric Power Engineering, South China University of Technology, Guangzhou, China, and the Director of the Energy Research Institute, South China University of Technology. His research interests include nonlinear adaptive control, mathematical morphology, evolutionary computation, power quality, and power system control and operation. He is a fellow of IET and InstMC and a Chartered Engineer.